communications biology

A Nature Portfolio journal

Article

https://doi.org/10.1038/s42003-025-09497-4

METTL3-mediated m6A modification of FDX1 confers resistance to cuproptosis and promotes hepatocellular carcinoma progression

Qian Jiang[1,7], Chen Peng[1,7], Wenhao Mao[2,7], Zhuo Yu[3], Yadan Feng[1], Yurui Li[4], Jialin Zhu[5], Jiao Zhao[1] ✉, Dan Liao[6] ✉ & Ting Sun[1] ✉

Cuproptosis, a copper-dependent cell death pathway, is emerging as a potential cancer treatment strategy. N6-methyladenosine (m6A), the predominant eukaryotic RNA modification, regulates various cell death mechanisms; however, its role in cuproptosis within hepatocellular carcinoma (HCC) remains unclear. Here, we found that METTL3 expression and m6A modification are upregulated during cuproptosis in HCC cells. Mechanistically, METTL3 mediated m6A modification of FDX1 mRNA, whereas the m6A reader FMR1 inhibited FDX1 translation. Consequently, METTL3 conferred resistance to cuproptosis by suppressing FDX1 protein expression in an m6A-FMR1-dependent manner. Knockdown or pharmacological inhibition of METTL3 sensitized HCC cells to elesclomol-Cu-induced cuproptosis and effectively suppressed HCC xenograft growth in vivo. Clinically, elevated METTL3 expression was associated with poor HCC prognosis, and the protein expression of METTL3 and FDX1 was negatively correlated in HCC tissues. In conclusion, our findings identify an METTL3-mediated m6A regulatory mechanism controlling cuproptosis sensitivity, revealing METTL3 inhibition as a promising therapeutic strategy for HCC.

Hepatocellular carcinoma (HCC) is a prevalent malignancy worldwide, accounting for more than 90% of all liver cancer cases. HCC typically arises in the context of cirrhosis, hepatitis B or C virus infection, or nonalcoholic steatohepatitis[1,2]. Despite recent advances in diagnosis and therapy, patients with advanced HCC remain resistant to current multikinase inhibitors or immune checkpoint inhibitors due to the high degree of genetic heterogeneity and a lack of specific therapeutically targetable mutations[3]. Accordingly, there is an urgent need to understand the underlying molecular mechanisms of HCC and develop effective approaches that address unmet needs in HCC therapy.

Cuproptosis is an emerging mode of cell death, a modality defined by Peter Tsvetkov et al. in 2022[4]. This process occurs through the direct binding of copper to lipoylated components involved in the tricarboxylic acid (TCA) cycle, which leads to the aggregation of lipoylated dihydrolipoamide S-acetyltransferase (DLAT) and the loss of iron-sulfur cluster proteins to induce proteotoxic stress and ultimately cell death[5]. Elesclomol is a significant copper ionophore that facilitates the transportation of excess intracellular Cu^{2+} to the mitochondria[6]. At this location, ferredoxin 1 (FDX1) functions as a reductase, reducing Cu^{2+} to its more toxic form, Cu^{+}. As a critical mediator of cuproptosis, FDX1 plays a pivotal role in the lipoylation of DLAT and the subsequent loss of Fe-S cluster proteins. Consequently, the loss of FDX1 function can render cells resistant to copper treatment. Recently, interest in exploiting cuproptosis for cancer therapy has increased[7,8]. Nevertheless, the molecular drivers of cancer cell evasion of cuproptosis remain to be elucidated.

N6-methyladenosine (m6A) is the most prevalent RNA modification in eukaryotic cells[9,10]. This modification is critical for various aspects of RNA function, including splicing, maturation, translation, and stability, making it

[1]Department of Clinical Laboratory, The First Affiliated Hospital of Zhengzhou University, Zhengzhou, China. [2]Department of Medical Oncology, The Affiliated Cancer Hospital of Zhengzhou University, Henan Cancer Hospital, Zhengzhou, China. [3]Department of Laboratory, Luoyang Maternal and Child Health Hospital, Luoyang, China. [4]Department of Pediatrics, The Fifth Medical Center of the PLA General Hospital, Beijing, China. [5]Information Technology Department of Zhengzhou Branch, China Merchants Bank, Zhengzhou, China. [6]Sun Yat-sen University Cancer Center, State Key Laboratory of Oncology in South China, Guangdong Provincial Clinical Research Center for Cancer, Collaborative Innovation Center for Cancer Medicine, Guangzhou, China. [7]These authors contributed equally: Qian Jiang, Chen Peng, Wenhao Mao. ✉e-mail: yfyzhaojiao@163.com; liaodan@sysucc.org.cn; sunting@zzu.edu.cn

essential for gene expression[11]. The m6A modification is reversible and catalyzed by corresponding enzymes, known as "writers" (methyltransferases), "erasers" (demethylases) and "readers"[12]. m6A, its regulatory enzymes, and reader proteins play critical roles in gene regulation. Targeting the regulatory proteins associated with m6A represents a promising therapeutic strategy for cancer[13–16]. A recent study demonstrated that m6A modification of LIPT1 inhibits bladder cancer progression by activating cuproptosis[17]. Nevertheless, the precise roles and molecular mechanisms underlying the m6A modification respond to cuproptosis in HCC remain unclear. A more comprehensive understanding of the role and underlying molecular mechanisms of m6A in cuproptosis will provide promising therapeutic targets for HCC and accelerate the development of HCC therapies.

In the present study, we found that the cuproptosis process is associated with m6A modification and METTL3 expression. Elevated METTL3 expression confers resistance to cuproptosis and protects HCC cells from cuproptotic cell death. Mechanistically, FDX1 is identified as a downstream target of METTL3, and FMR1 recognizes the m6A modification of FDX1 mRNA, leading to the inhibition of its translation efficiency. Consequently, METTL3-mediated m6A modification results in downregulation of FDX1 expression, thereby inhibiting cuproptosis in HCC. Moreover, knockdown or pharmacological inhibition of METTL3 sensitized HCC cells to elesclomol-Cu-induced cuproptosis and effectively suppressed HCC xenograft growth in vivo. In conclusion, these findings demonstrate the significance of m6A modification as a distinct mechanism regulating cuproptosis and highlight a potential therapeutic strategy for HCC by targeting METTL3 to enhance cuproptosis.

Results

m6A modification is increased during cuproptosis in HCC cells

Elesclomol is a well-established copper ionophore that functions as a cuproptosis agonist. To investigate whether cuproptosis is involved in elesclomol-induced cell death in HCC cells, we first examined the viability of HCC cells treated with elesclomol and copper at a 1:1 ratio (elesclomol-Cu, ES-Cu). Hep3B and Huh7 cells were exposed to a range of concentrations of elesclomol-Cu for 24 or 48 h, and significant inhibition of cell survival was observed in a dose-dependent manner (Fig. 1A, B). The results of the 5-ethynyl-2'-deoxyuridine (EdU) assay also confirmed that the proliferative capacity of HCC cells was diminished following treatment with elesclomol-Cu (Fig. 1C, D). Furthermore, cell death induced by elesclomol-Cu was identified by flow cytometry in Hep3B and Huh7 cells (Fig. 1E, F). These results demonstrated that elesclomol-Cu had an adverse effect on cell viability and induced cell death in HCC cells. We subsequently investigated whether the cell death induced by elesclomol-Cu was attributable to cuproptosis. Cell death could be prevented by cotreatment with tetrathiomolybdate (TTM, a cuproptosis inhibitor), but not with ferrostatin-1 (Fer-1, a ferroptosis inhibitor), 3-methyladenine (3-MA, an autophagy inhibitor), or Z-VAD-fmk (a caspase inhibitor) (Fig. 1G, H), indicating that cuproptosis occurs during elesclomol-Cu treatment in HCC cells.

An increasing amount of evidence has revealed that m6A plays a regulatory role in gene expression, influencing a range of programmed cell death processes[18]. To determine whether m6A modification affects cuproptosis, we analyzed m6A modification in HCC cells following elesclomol-Cu treatment. The m6A dot blot assay and EpiQuik m6A RNA methylation quantification both demonstrated that the m6A modification levels were elevated in Huh7 and Hep3B cells following treatment with elesclomol-Cu. Moreover, the increase in the m6A modification level was reversed by TTM treatment (Fig. 1I-J). Together, these results indicate that elesclomol-Cu-induced cuproptosis is accompanied by increased m6A modification levels in HCC cells.

METTL3 mediates the upregulation of m6A modification during cuproptosis

m6A modification is a reversible process, which is added by m6A "writers"; such as METTL3, METTL14, and WTAP, and removed by "erasers"; such as FTO and alkB homolog 5 (ALKBH5). To determine the potential causes of the observed increase in m6A modification in cuproptotic HCC cells, we analyzed the expression levels of METTL3, METTL14, WTAP, FTO and ALKBH5 following elesclomol-Cu treatment. The protein and mRNA levels of METTL3 were markedly elevated in HCC cells after ES-Cu treatment, while the other writers and erasers did not exhibit notable alterations (Fig. 2A-C). Moreover, the increased level of METTL3 was inhibited by treating HCC cells with TTM (Fig. 2A-C). Additionally, time-course experiments revealed that METTL3 protein expression and m6A modification levels increased significantly in a time-dependent manner following exposure to cuproptotic stimuli (Supplementary Fig. 1A, B). Since METTL3 is a pivotal m6A writer, we postulated that elevated levels of METTL3 might drive the increased m6A modification observed during HCC cuproptosis. We subsequently designed and synthesized METTL3 shRNAs to perform loss-of-function experiments. As anticipated, METTL3 knockdown resulted in a notable reduction in m6A modification levels in elesclomol-Cu-treated HCC cells (Fig. 2D-F). In conclusion, these results demonstrated that METTL3 is responsible for m6A modification during HCC cuproptosis.

Considering that METTL3 expression is upregulated during cuproptotic cell death in HCC, we speculated that METTL3 might promote cuproptosis in HCC cells. Unexpectedly, METTL3 knockdown enhanced the growth inhibition, decreased cell proliferation, and intensified ES-Cu-induced cell death (Fig. 2G-K). These findings suggest that elesclomol-Cu-induced METTL3 upregulation may constitute a protective mechanism that confers resistance to cuproptosis in HCC cells.

METTL3 inhibits FDX1 protein expression via m6A modification

To gain further insight into the molecular mechanism by which METTL3 regulates cuproptosis in HCC cells, RNA sequencing (RNA-Seq) was conducted on METTL3-knockdown and control cells. Unexpectedly, no cuproptosis-related genes, such as FDX1, LIAS, LIPT1, DLD, DLAT, PDHA1 or PDHB, were identified among these genes (Fig. 3A, B). These findings indicate that METTL3-mediated m6A modification does not directly regulate the transcription of cuproptosis-related genes but may act through a posttranscriptional regulatory pathway. Given that METTL3 knockdown enhances elesclomol-Cu-induced cuproptotic cell death, and that elesclomol specifically binds to FDX1 and suppresses Fe-S cluster biosynthesis, we sought to determine whether FDX1 functions as a downstream mediator of METTL3 in the regulation of cuproptosis.

A methylated RNA immunoprecipitation (MeRIP)-qPCR assay was employed to detect m6A modification of FDX1. Our findings revealed that METTL3 knockdown resulted in a notable reduction in the m6A modification level of FDX1 mRNA in HCC cells (Fig. 3C), whereas METTL3 overexpression had the opposite effect (Fig. 3D). The m6A modification sites in FDX1 mRNA were subsequently analyzed using the SRAMP prediction program (www.cuilab.cn/sramp), which identified three potential m6A modification sites with very high confidence: sites 602 and 655 in the coding sequence region and site 820 in the 3'-untranslated region (3'-UTR) of the FDX1 transcript (Fig. 3E). Subsequent MeRIP-qPCR analysis using specific primers revealed that site 820 was the predominant m6A modification site in the FDX1 transcript (Fig. 3F). To confirm m6A modification at site 820, an FDX1-820-Mut plasmid was constructed by mutating 820 A to T (Fig. 3E). The MeRIP-qPCR results demonstrated that METTL3 overexpression promotes the m6A modification of FDX1-WT but not FDX1-820-Mut (Fig. 3G). These findings suggest that METTL3 mediates m6A modification of FDX1 mRNA at site 820.

The effect of METTL3-mediated m6A modification on FDX1 expression was then examined. METTL3 knockdown did not result in notable alterations in FDX1 mRNA expression in Huh7 and Hep3B cells (Fig. 3H). However, it led to a considerable increase in FDX1 protein levels (Fig. 3I). Consistent with these findings, we also observed minimal alterations in FDX1 mRNA levels but a decrease in FDX1 protein levels in cells with METTL3 overexpression (Fig. 3J, K). RNA degradation experiments confirmed that METTL3 had no effect on the stability of FDX1 mRNA

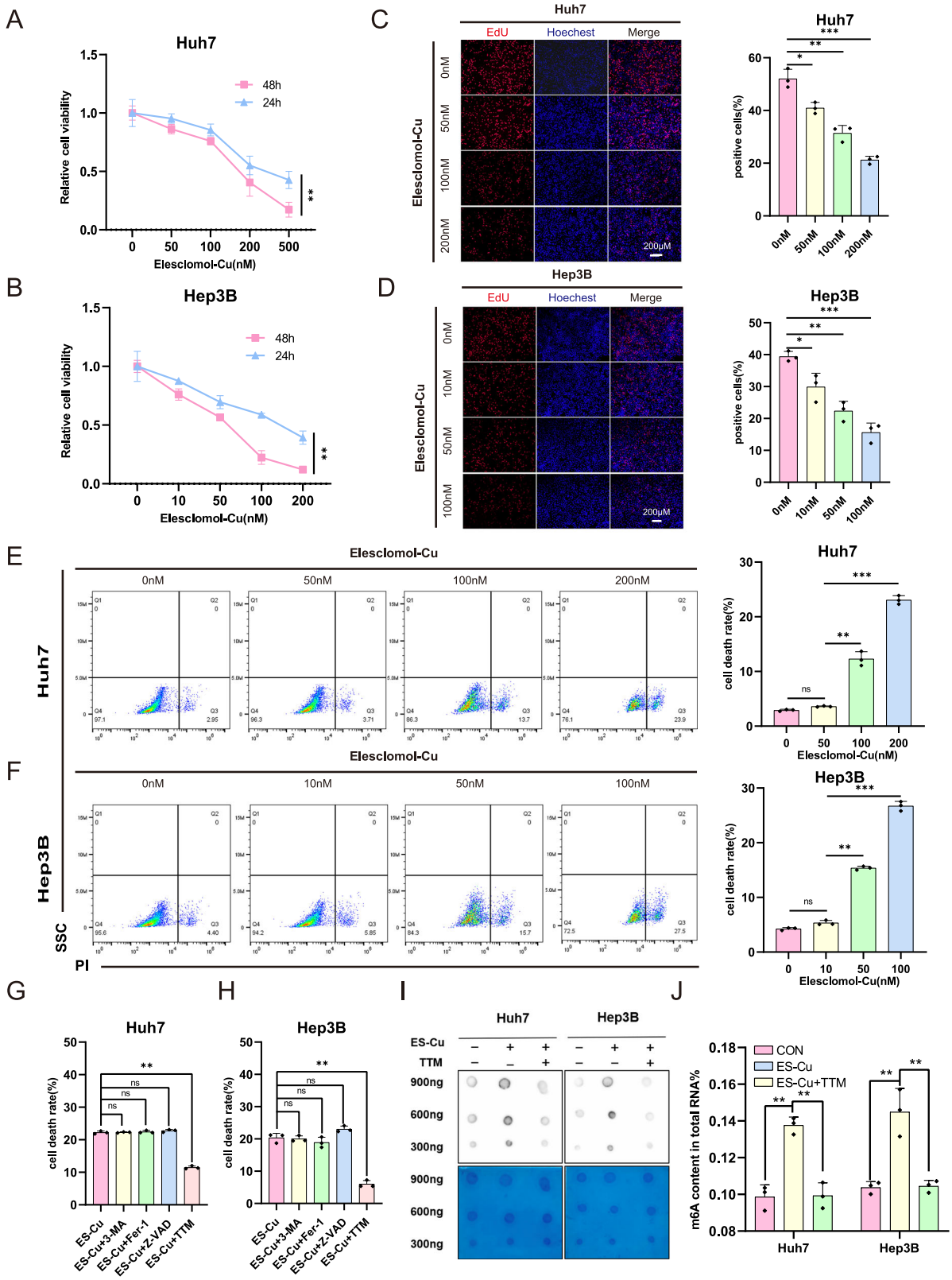

Fig. 1 | Increased m6A modification during cuproptosis in HCC cells. Survival analysis of Huh7 (**A**) and Hep3B (**B**) cells treated with the indicated concentrations of ES-Cu after 24 or 48 h. Proliferation of Huh7 (**C**) and Hep3B (**D**) cells treated with indicated concentrations of ES-Cu for 48 h, assessed by EdU labeling. Scale bars: 200 μm. Cell death rates in Huh7 (**E**) and Hep3B (**F**) cells treated with indicated concentrations of ES-Cu for 48 h, measured by flow cytometry. Cell death rates in Huh7 (**G**) and Hep3B (**H**) cells treated for 48 h with ES-Cu (Huh7: 200 nM; Hep3B: 100 nM) alone or combined with inhibitors: 3-MA (0.2 μM), Ferrostatin-1 (100 nM), Z-VAD (1 μM), or TTM (1 μM), analyzed by flow cytometry. **I** Dot blot analysis of m6A modification levels in Huh7 and Hep3B cells treated with ES-Cu or TTM for 48 h. **J** Quantification of m6A modification levels using the EpiQuik m6A RNA Methylation Quantification Kit in cells treated as in (**I**). Data are presented as mean ± SD. *$p < 0.05$; **$p < 0.01$; ***$p < 0.001$; ns, not significant.

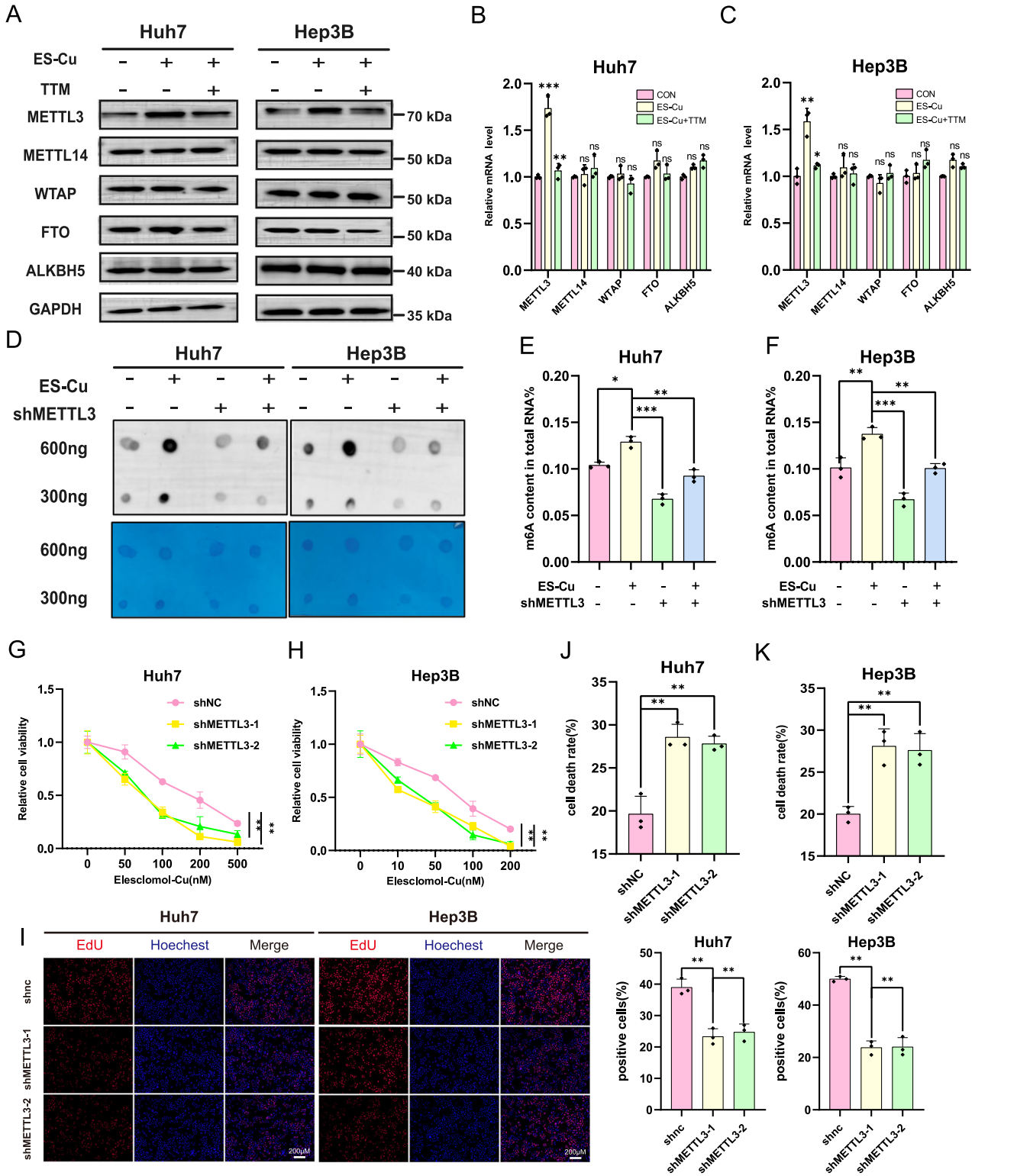

Fig. 2 | METTL3 mediates m6A upregulation during cuproptosis in HCC cells. **A** Western blot analysis of indicated proteins in Huh7 and Hep3B cells treated with or without ES-Cu (Huh7: 200 nM; Hep3B: 100 nM) and/or TTM (1 μM) for 48 h. Relative mRNA levels of indicated genes in Huh7 (**B**) and Hep3B (**C**) cells treated as in (**A**), analyzed by qRT-PCR. **D** The level of m6A modification was detected by dot blot. Quantification of m6A modification levels in Huh7 (**E**) and Hep3B (**F**) cells, using the EpiQuik m6A RNA Methylation Quantification Kit. Survival analysis of Huh7 (**G**) and Hep3B (**H**) cells treated with ES-Cu for 48 h. **I** Proliferation of Huh7 and Hep3B cells treated with ES-Cu for 48 h, assessed by EdU labeling. Scale bars: 200 μm. Cell death rates in Huh7 (**J**) and Hep3B (**K**) cells treated with ES-Cu for 48 h, quantified by flow cytometry. Data are presented as mean ± SD. *$p < 0.05$; **$p < 0.01$; ***$p < 0.001$; ns, not significant.

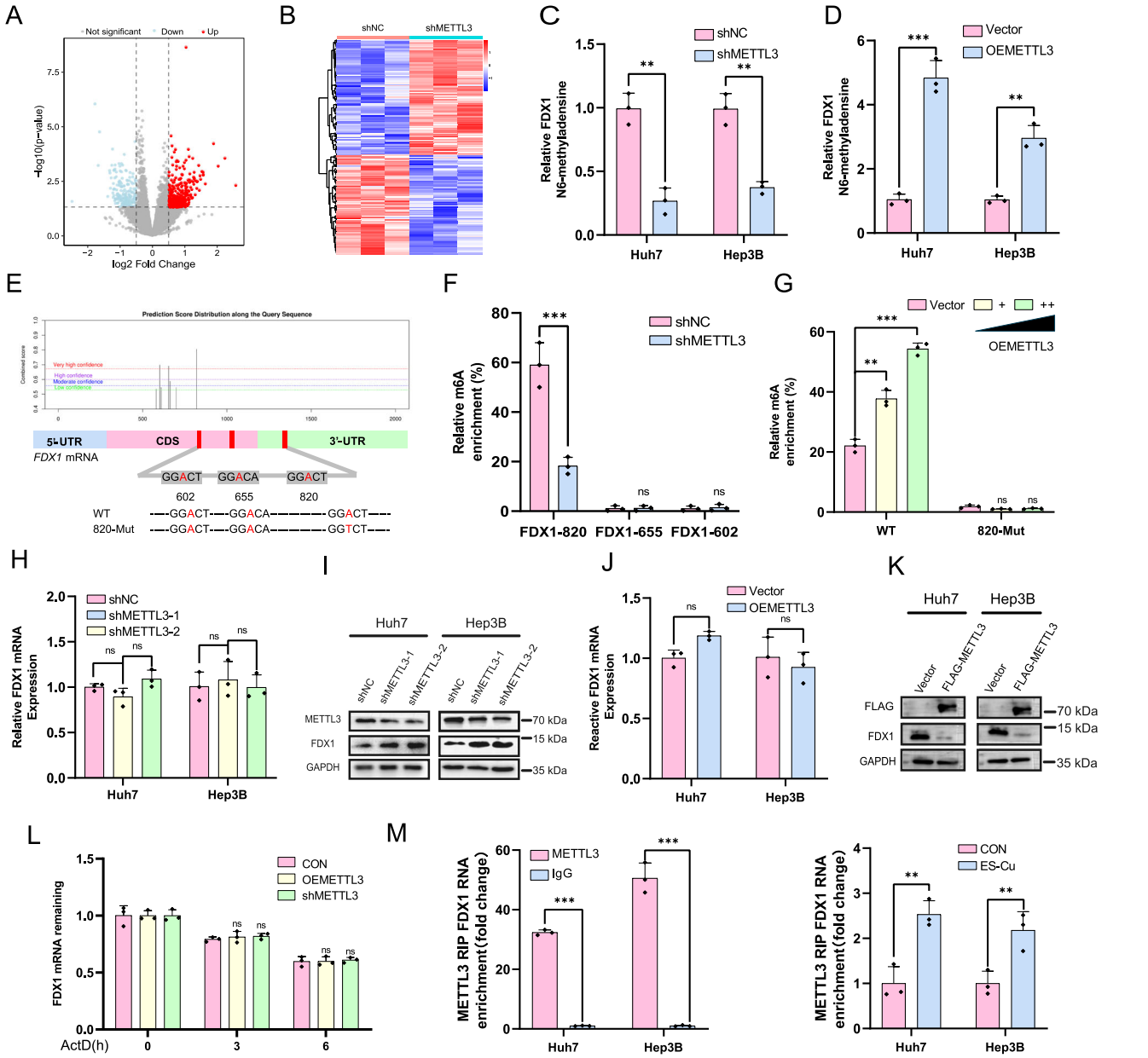

Fig. 3 | METTL3 inhibits FDX1 protein expression via m6A modification. RNA sequencing analysis of differentially expressed genes (DEGs) in Huh7 cells expressing indicated shRNAs and treated with ES-Cu (200 nM, 48 h) (fold change >1.5 and p-value < 0.05). **A** Volcano plot; **B** Heatmap of enriched DEGs. **C**, **D** MeRIP-qPCR assay analysis of m6A levels on FDX1 mRNA in the indicated cell lines. **E** Predicted m6A motifs in FDX1 mRNA (SRAMP server: http://www.cuilab.cn/sramp). Schematic of the FDX1-820-mut construct is shown. **F** MeRIP-qPCR assay analysis of m^{6}A levels at specific sites of FDX1 mRNA in Huh7 cells. **G** MeRIP-qPCR assay analysis of m6A levels at site 820 of FDX1 mRNA in Huh7 cells. **H**, **J** FDX1 mRNA expression in indicated cell lines, analyzed by qRT-PCR. **I**, **K** Western blot analysis of METTL3 and FDX1 protein expression in indicated cell lines. **L** FDX1 mRNA stability in HCC cells treated with actinomycin D (ActD; 10 μg/mL), assessed by qRT-PCR. **M** METTL3-FDX1 mRNA interaction confirmed by RIP-qPCR in Huh7 and Hep3B cells. ES-Cu enhances METTL3-FDX1 mRNA interaction. Data are presented as mean ± SD. *p < 0.05; **p < 0.01; ***p < 0.001; ns, not significant.

(Fig. 3L). Moreover, RIP-qPCR was employed to confirm the interaction between METTL3 and FDX1 mRNA. These findings demonstrated that ES-Cu treatment significantly increased the enrichment of FDX1 mRNA in METTL3 immunoprecipitates, indicating enhanced METTL3-FDX1 RNA binding upon cuproptosis induction (Fig. 3M). In conclusion, these data collectively indicate that METTL3-mediated m6A modification negatively regulates effect on FDX1 protein expression without affecting mRNA transcription or mRNA stability.

The m6A reader FMR1 represses FDX1 translation in an m6A-dependent manner

RNA m6A modifications are recognized by m6A-binding proteins (readers), which play pivotal roles in enabling methylated mRNAs to perform diverse biological functions. To determine which reader protein is involved in recognizing the m6A modification of FDX1, an unbiased expression screen was conducted on the five most common reader proteins: YTHDFl, YTHDF2, YTHDF3, YTHDCl and YTHDC2.

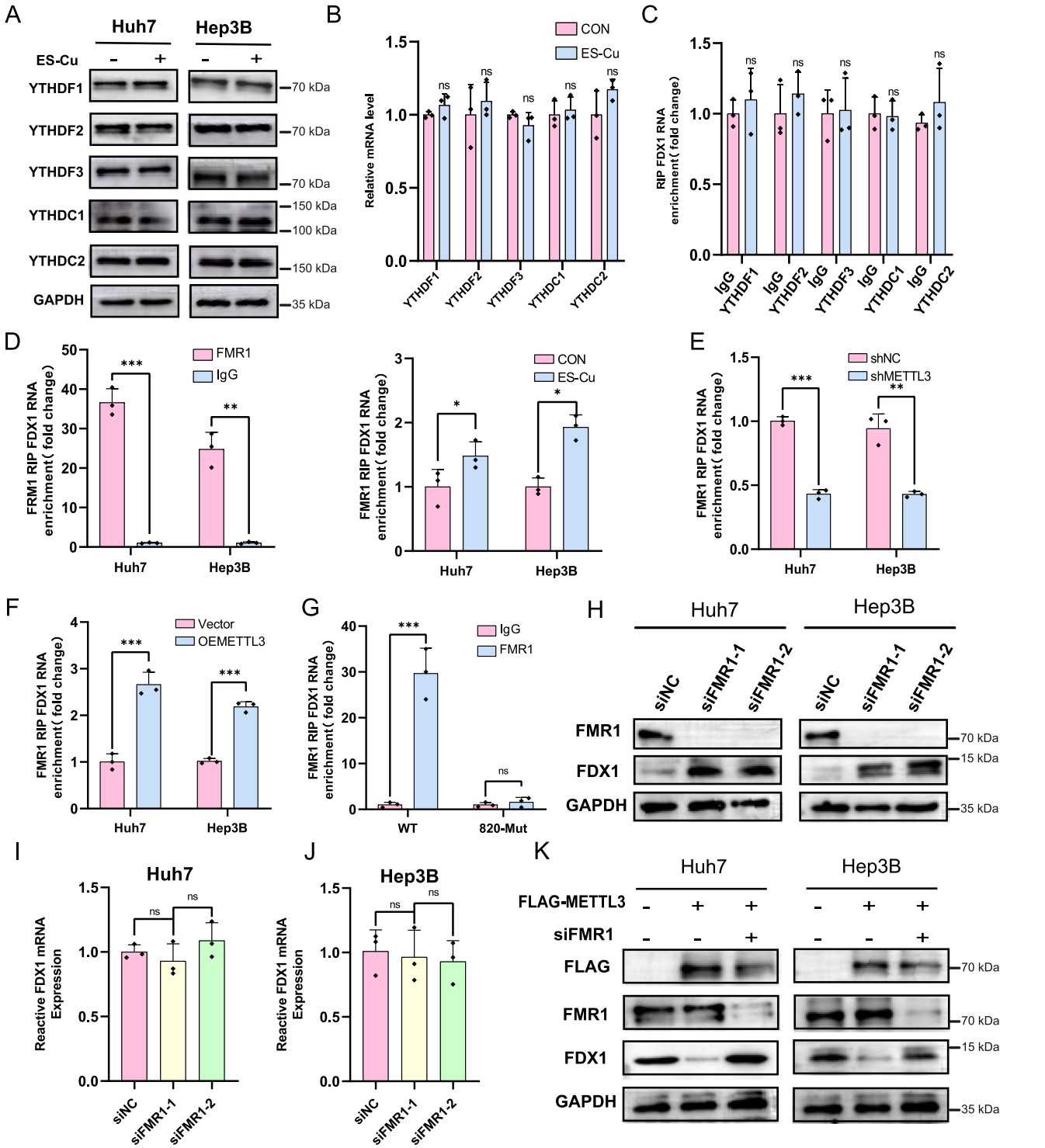

Fig. 4 | The m6A reader FMR1 represses FDX1 translation in an m6A-dependent manner. A Western blot analysis of m6A reader protein levels in Huh7 and Hep3B cells treated with or without ES-Cu (Huh7: 200 nM; Hep3B: 100 nM). **B** Relative mRNA expression of m6A readers in Huh7 and Hep3B cells. **C** RIP-qPCR analysis showing no significant interaction between FDX1 mRNA and other m6A readers in Huh7 and Hep3B cells. **D** RIP-qPCR confirmation of FMR1–FDX1 mRNA interaction in Huh7 and Hep3B cells; ES-Cu enhances this binding. Effect of METTL3 knockdown (**E**) or METTL3 overexpression (**F**) on FMR1–FDX1 mRNA interaction, assessed by RIP-qPCR. **G** RIP-qPCR validation of FMR1 interaction with the FDX1-WT or FDX1-820 mutant mRNA. **H** Western blot analysis of FDX1 protein expression in control and FMR1-knockdown cells. **I**, **J** qRT-PCR analysis of FDX1 mRNA expression in control and FMR1-knockdown cells. **K** Western blot analysis of indicated proteins in Huh7 and Hep3B cells. Data are presented as mean ± SD. *p < 0.05; **p < 0.01; ***p < 0.001; ns, not significant.

Unexpectedly, the protein or mRNA expression of the five readers exhibited minimal alterations following treatment with elesclomol-Cu (Fig. 4A, B). Additionally, the results of the RIP-qPCR assays revealed that there was no considerable interaction between these readers and FDX1 mRNA (Fig. 4C). Given that METTL3 negatively regulates FDX1 protein expression at the posttranscriptional level without affecting its mRNA stability, we hypothesized that METTL3-mediated m6A modification may suppress FDX1 mRNA translation.

FMR1 has been identified as a sequence-dependent m6A reader that colocalizes with m6A on mRNAs and preferentially interacts with m6A-containing mRNAs in vivo[19]. FMR1 has been reported to stall ribosomal translocation during elongation as part of a complex containing target mRNAs and ribosomes, analogous to the function of the Signal Recognition Particle (SRP)[20]. We next investigated whether FMR1 regulates FDX1 expression. First, ES-Cu treatment did not alter FMR1 protein expression (Supplementary Fig. 2A). Furthermore, neither FMR1 knockdown nor FMR1 overexpression significantly affected global m6A abundance (Supplementary Fig. 2B). RIP-qPCR confirmed an interaction between FMR1 and FDX1 mRNAs, and this binding affinity was enhanced by ES-Cu treatment (Fig. 4D). Additionally, METTL3 modulated the binding between FDX1 mRNA and FMR1 (Fig. 4E, F). Collectively, these data support a model in which FMR1 functions primarily as a reader protein to modulate the fate of m6A-modified transcripts rather than influencing m6A addition or removal.

As we previously demonstrated that METTL3 methylates FDX1 mRNA at site 820, we employed the FDX1-mut variant to assess the functional significance of this site for FMR1 binding. As expected, the FDX1-820-Mut variant disrupted FMR1 binding to FDX1 mRNA (Fig. 4G). Furthermore, FMR1 knockdown increased FDX1 protein expression (Fig. 4H), without affecting FDX1 mRNA levels (Fig. 4I, J). This finding was consistent with the established function of FMR1 in repressing protein translation[19]. Additionally, FMR1 knockdown partially rescued the down-regulation of FDX1 protein levels caused by METTL3 overexpression (Fig. 4K). Collectively, these data indicate that FMR1 suppresses FDX1 translation in an m6A-dependent manner.

METTL3 confers resistance to cuproptosis by targeting FDX1

Our previous studies demonstrated that METTL3 protects HCC cells from cuproptotic cell death; thus, we wondered whether METTL3 confers resistance to cuproptosis by regulating FDX1 expression. METTL3 knockdown resulted in the sensitization of HCC cells to elesclomol-Cu treatment. Tetrathiomolybdate (TTM), a cuproptosis inhibitor, suppressed cuproptosis in METTL3-knockdown cells, indicating that METTL3 is involved in cuproptosis (Fig. 5A, B). Furthermore, cuproptosis induced by METTL3 knockdown was reversed by FDX1 knockdown (Fig. 5A, B). EdU assays further confirmed that METTL3 knockdown diminished the proliferation ability of HCC cells, which was rescued by FDX1 knockdown (Fig. 5C, D). The flow cytometry data corroborated these findings, demonstrating that FDX1 knockdown attenuated HCC cell death induced by METTL3 knockdown (Fig. 5E, F). Given that protein lipoylation represents the key element of cuproptosis, we also evaluated protein lipoylation using a lipoic acid (LA)-specific antibody, which serves as an indicator of DLAT lipoylation. The results demonstrated that the reduction in DLAT lipoylation mediated by METTL3 overexpression was reversed by the exogenous expression of FDX1 (Fig. 5G). Collectively, these data collectively indicate that METTL3 protects HCC cells from cuproptotic cell death by targeting FDX1.

Targeting METTL3 enhances the anticancer effects of elesclomol in HCC

Considering the established link between elesclomol and cuproptosis, the clinical anticancer potential of elesclomol has attracted renewed attention. Since our findings suggest that METTL3 confers resistance to cuproptosis, we further investigated whether METTL3 affects the anticancer activity of ES-Cu in vivo. Huh7 cells overexpressing METTL3 or FDX1 were injected subcutaneously into BALB/c nude mice, followed by ES-Cu treatment (10 mg/kg) (Fig. 6A). Tumor growth was markedly inhibited in mice receiving ES-Cu treatment in the FDX1 overexpressing group, as indicated by a reduced tumor volume (Fig. 6B, C). Conversely, METTL3 overexpression significantly attenuated the efficacy of ES-Cu in suppressing tumor growth, thereby mitigating the effects of FDX1 overexpression. Immunofluorescence staining of tumor sections revealed reduced DLAT aggregation in the METTL3 overexpressing group and increased DLAT aggregation in the FDX1 overexpressing group (Fig. 6D). Conversely, the expression of the cell proliferation marker Ki67 was greater in the METTL3 overexpressing group than in the control group, which was reversed by FDX1 overexpression (Fig. 6E). These findings indicate that METTL3 plays a crucial role in determining cuproptosis. Furthermore, the decreased sensitivity to elesclomol-Cu therapy observed in METTL3-overexpressing cells was associated with cuproptosis resistance.

Additionally, we investigated whether inhibition of METTL3 could attenuate the anticancer activity of elesclomol-Cu in tumor xenografts (Fig. 6F). STM2457, a highly selective METTL3 inhibitor, has been reported for use in acute leukemia[21]. We found that STM2457 sensitized cells to elesclomol-Cu treatment in vivo, as indicated by a reduction in tumor volume (Fig. 6G, H). Immunofluorescence staining of tumor sections revealed that STM2457 intensified cell sensitivity to elesclomol-Cu therapy was associated with increased DLAT aggregation (Fig. 6I). Additionally, treatment with the METTL3 inhibitor (STM2457) and elesclomol-Cu reduced Ki67 expression in tumor tissues (Fig. 6J). In conclusion, the preclinical animal studies presented here support the hypothesis that targeting METTL3 significantly enhances the anticancer activity of elesclomol-Cu. The combination of a METTL3 inhibitor with elesclomol-Cu, therefore, represents a promising candidate therapy for HCC.

METTL3 expression is negatively correlated with FDX1 in patients with HCC

To evaluate the expression of METTL3 in HCC, we analyzed gene expression using a web-based tool (GEPIA, Gene Expression Profiling Interactive Analysis, http://gepia.cancer-pku.cn/)[22] according to the TCGA database. The results demonstrated that METTL3 expression was significantly elevated in human HCC tissues. Furthermore, elevated METTL3 expression was significantly associated with poor overall and disease-free survival rates in patients with HCC (Fig. 7A-C). These results were subsequently validated in a real-world setting. METTL3 expression was determined in 48 pairs of HCC and adjacent normal tissues using IHC staining analysis. METTL3 protein expression was upregulated in HCC tissues (Fig. 7D) and was negatively correlated with FDX1 expression (Fig. 7E). Moreover, western blotting confirmed the inverse correlation between METTL3 and FDX1 protein expression level in HCC tissues and cell lines (Fig. 7F, G). Additionally, IHC staining analysis revealed no significant difference in FMR1 expression between HCC and adjacent normal tissues (Supplementary Fig. 3A), suggesting that FMR1 may not play a direct role in regulating HCC progression. Correlation analysis revealed no statistically significant associations between FMR1 and either METTL3 or FDX1 expression levels (Supplementary Fig. 3B). The lipoylation of DLAT is a well-established marker of cuproptosis; therefore, we evaluated protein lipoylation using a lipoic acid (LA)-specific antibody, which serves as an indicator of DLAT lipoylation and cuproptosis[23]. Correlation analysis revealed that LA levels were negatively correlated with METTL3 expression but positively correlated with FDX1 expression. There was no statistically significant association between LA and FMR1 expression (Supplementary Fig. 4A, B).

Taken together, these findings indicate that METTL3 is upregulated in HCC and that elevated METTL3 expression predicts poor prognosis in patients with HCC. These findings, combined with our previous results, suggest that targeting METTL3 to enhance cuproptosis represents a potential therapeutic strategy for HCC.

Discussion

Cuproptosis is a specific copper-mediated cell death pathway that differs from apoptosis, pyroptosis, ferroptosis and necroptosis[24]. It has been reported that m6A contributes to the regulation of various forms of cell death in cancer[18,25], but few studies have investigated the function of m6A modification on cuproptosis in cancer cells. Accordingly, the mechanisms underlying how m6A affects cuproptosis remain largely unclear. In this study, we used elesclomol-Cu to treat HCC cells, thereby demonstrating its capacity to induce cuproptotic cell death. Furthermore, we observed that

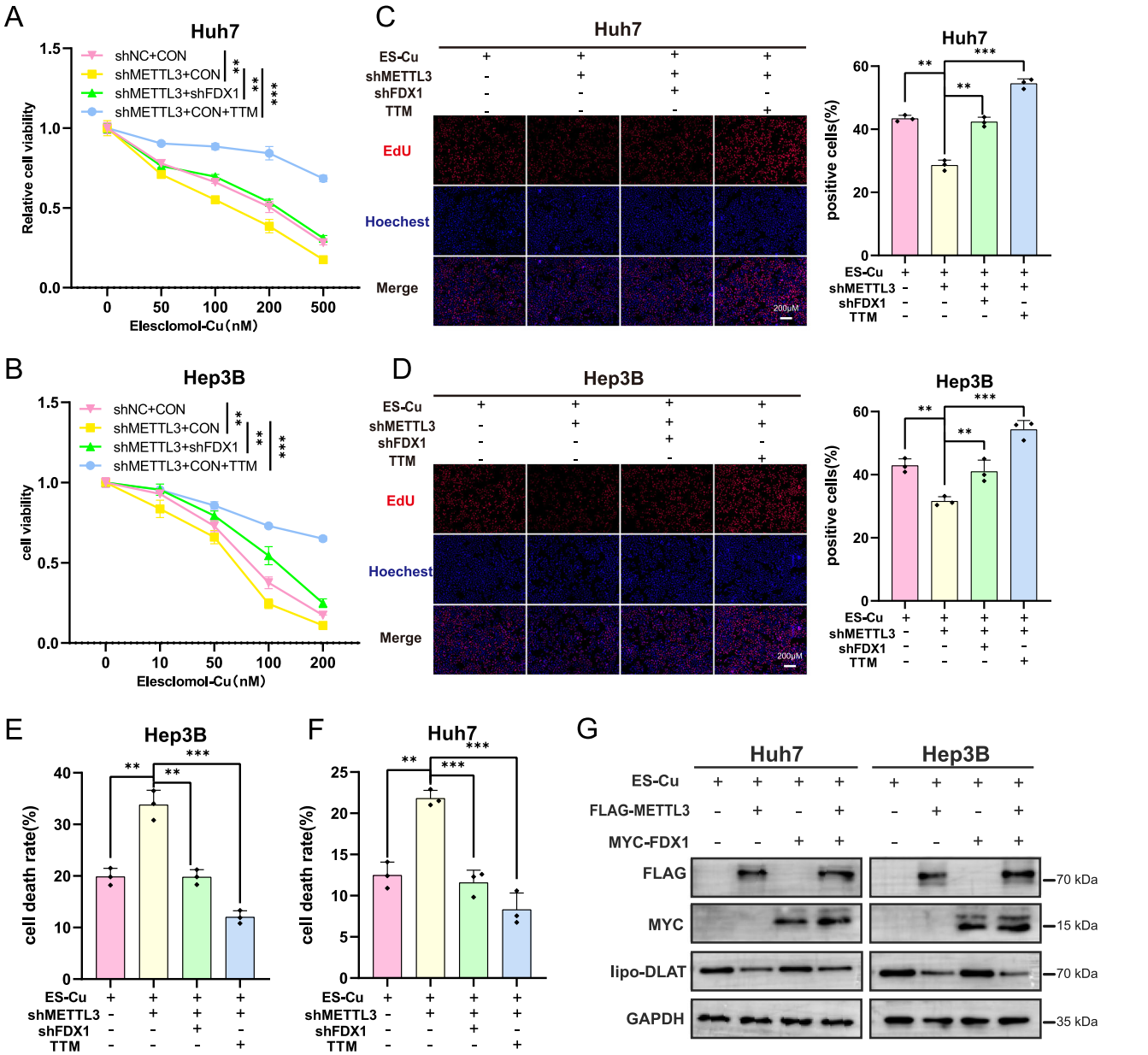

Fig. 5 | METTL3 inhibits cuproptosis by targeting FDX1. Survival analysis of Huh7 (**A**) and Hep3B (**B**) cells expressing indicated shRNAs under different treatments. Proliferation capacity of Huh7 (**C**) and Hep3B (D) cells assessed by EdU assay. Scale bars: 200 μm. Cell death rate of Huh7 (**E**) and Hep3B (**F**) cells quantified by flow cytometry. **G** Representative Western blot analysis of lipoylated DLAT (lipo-DLAT) expression in control or Flag-METTL3 expressing HCC cells transfected with or without MYC-FDX1. Data are presented as mean ± SD. *p < 0.05; **p < 0.01; ***p < 0.001; ns, not significant.

elesclomol-Cu increased METTL3 expression and m6A modification in HCC cells. Therefore, we speculated that METTL3-mediated m6A modification might be involved in the regulation of cuproptosis.

METTL3, a major RNA N6-adenosine methyltransferase, has been the subject of extensive investigation in various cancers[21,26–29], including HCC[30–32]. Targeting METTL3 represents a promising strategy for cancer therapy, as evidenced by preclinical studies[33–35]. For example, a small-molecule drug known as STM2457 targets METTL3 and has been found to elicit therapeutic effects in myeloid leukemia[21]. Nevertheless, the development of METTL3-targeting drugs remains in its early stage. METTL3-mediated m6A modification has been demonstrated to be involved in the regulation of ferroptosis[36,37]. Nevertheless, the precise function and mechanism of METTL3 in cuproptosis remain largely unknown. This study demonstrates the critical role of METTL3 in protecting HCC cells from cuproptotic cell death. Inhibition of METTL3 enhances the antitumor effects of elesclomol-Cu in HCC.

In this study, we revealed that elesclomol-Cu upregulated METTL3 expression while inducing cuproptosis, although the mechanism involved remains unclear. Studies have shown that the expression of METTL3 is regulated through various mechanisms, including transcriptional regulation, posttranscriptional regulation, and posttranslational modifications. In pancreatic cancer, cigarette smoke condensate induces hypomethylation of the METTL3 promoter and, subsequently, the recruitment of the transcription factor NFIC to induce METTL3 overexpression[38]. Additionally, p300 mediates histone H3 acetylation at lysine 27 (H3K27ac)[39] and histone H3 lactylation at lysine 18 (H3K18la)[37], which promote METTL3 transcription. MicroRNAs, including miR-33a, miR-186, miR-4429, miR-600, and let-7g[40–44], have been proposed to regulate METTL3 by targeting

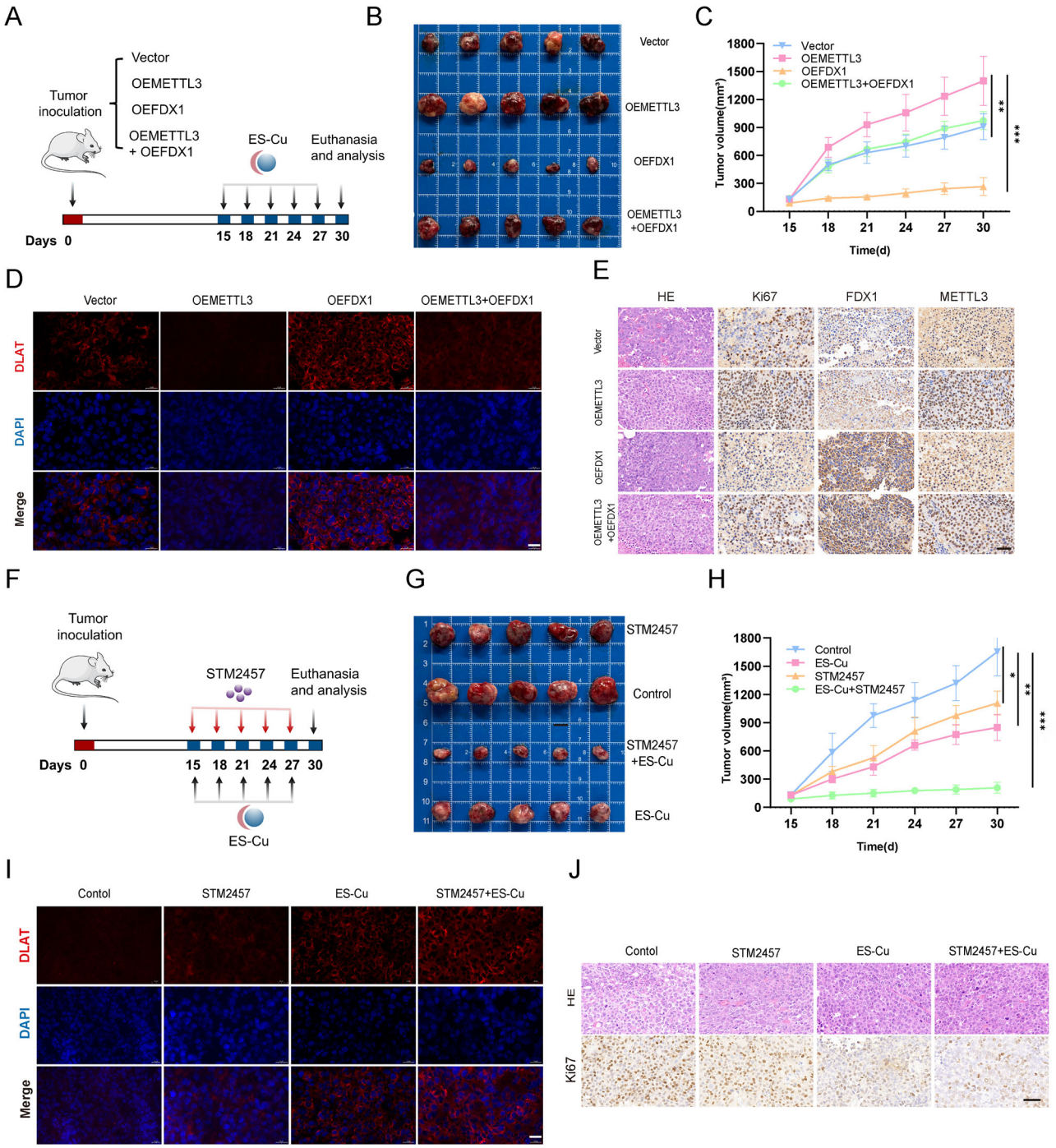

Fig. 6 | Targeting METTL3 enhances the anti-tumor efficacy of elesclomol in HCC. A Schematic of subcutaneous implantation of indicated Huh7 cells in BALB/c nude mice, followed by ES-Cu treatment (10 mg/kg). **B** Subcutaneous tumor models established with indicated Huh7 cells (n = 5). **C** Quantification of tumor growth in models from (**B**). **D** Immunofluorescence analysis of DLAT in tumor tissues (Scale bar: 20 μm). **E** Representative H&E staining and IHC for Ki67, FDX1, and METTL3 in tumor tissues (Scale bars: 50 μm). **F** Scheme illustrating combined treatment with METTL3 inhibitor STM2457 (30 mg/kg) and ES-Cu (10 mg/kg) in BALB/c nude mice. **G** Xenograft experiments were conducted with PBS, STM2457, ES-Cu, and ES-Cu + STM2457 treatments. Tumors were collected and photographed (n = 5). **H** Quantification of tumor growth in models from (**G**). **I** Immunofluorescence analysis of DLAT in tumor tissues (Scale bar: 20 μm). **J** Representative H&E staining and IHC for Ki67 in tumor tissues (Scale bars: 50 μm). Data represent mean ± SD. *p < 0.05; **p < 0.01; ***p < 0.001; ns, not significant.

METTL3 mRNA. Moreover, posttranslational modifications, including SUMOylation[45], lactylation[46], ubiquitination[47], and acetylation[48], are also involved in the regulation of METTL3. Therefore, the regulation of METTL3 is complex, and the mechanisms by which cuproptosis stress increases METTL3 expression need further investigation.

FDX1 plays a pivotal role in copper-induced cell death by functioning as a reductase that reduces Cu^{2+} to Cu^{+}. Previous studies have demonstrated that elevated FDX1 expression can diminish HCC cell viability and render HCC cells susceptible to Cu^{2+}, suggesting a correlation between FDX1 and cuproptosis in HCC[49]. Moreover, FDX1 downregulation has been

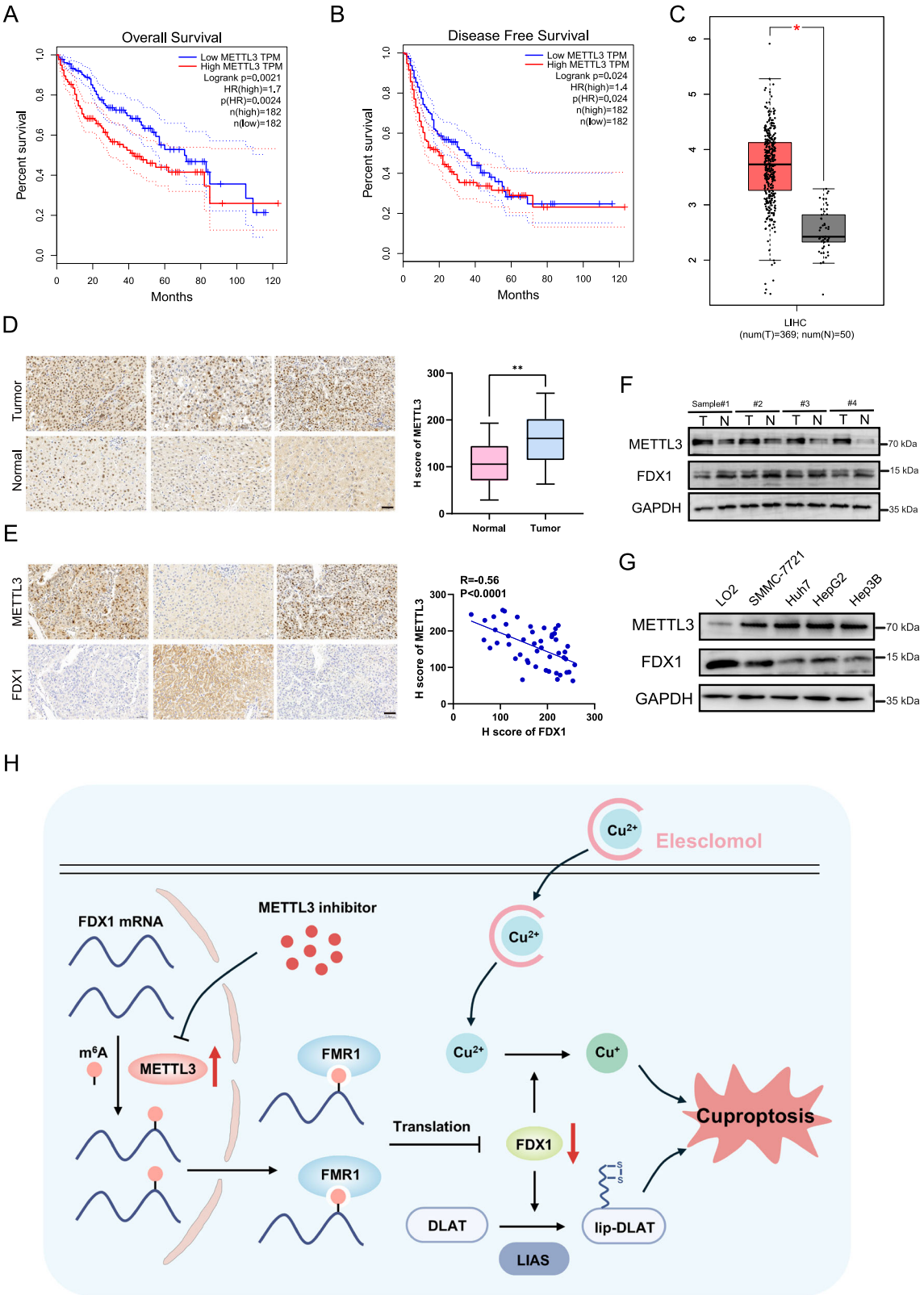

Fig. 7 | METTL3 expression is negatively correlated with FDX1 in HCC patients. **A**, **B** Kaplan–Meier analysis of overall survival (OS) and disease-free survival (DFS) in TCGA-LIHC cohort (n = 364) stratified by METTL3 expression (high vs. low). **C** METTL3 expression in TCGA-LIHC cohort (n = 364). **D** Representative IHC staining of METTL3 in HCC and adjacent normal tissues (Scale bars, 50μm). **E** IHC staining of FDX1 and METTL3 in the collected HCC tissues (Scale bars, 50μm). **F** Western blot analysis of FDX1 and METTL3 expression in paired tumor (T) and adjacent normal (N) tissues from 4 HCC patients. **G** Western blot analysis of FDX1 and METTL3 expression in HCC cell lines (LO2, SMMC-7721, HepG2, Huh7, and Hep3B). **H** The proposed model illustrates the regulation of cuproptosis sensitivity by METTL3/FDX1 signaling in HCC cells. Data are presented as mean ± SD. *p < 0.05; **p < 0.01; ***p < 0.001; ns, not significant.

demonstrated to activate mitophagy and the PI3K/AKT signaling pathway, thereby promoting HCC progression through the induction of ROS production[50]. Nevertheless, systematic experimental studies on FDX1 in HCC are still lacking. In this study, we identified FDX1 as a downstream target of METTL3 in HCC, further expanding the understanding of METTL3's regulatory targets in hepatocellular carcinoma. A previous study reported that METTL16, an atypical methyltransferase, promotes cuproptosis through m6A modification of FDX1 mRNA in gastric cancer[51]. Researchers discovered that METTL16 facilitates FDX1 accumulation through m6A modification at site 602 on FDX1 transcripts. However, our present study revealed that METTL3 mediates the m6A methylation of FDX1 at a different site, site 820 on FDX1 transcripts. Moreover, METTL3-mediated m6A methylation inhibits FDX1 translation in an FMR1-dependent manner. Therefore, METTL3-mediated m6A modification of FDX1 inhibits cuproptosis in HCC. These studies indicate that the impact of m6A on cuproptosis may be contingent upon the cell type and disease model. Since m6A modification affects various aspects of RNA, including splicing, maturation, translation and stability, it can either positively or negatively regulate gene expression. Consequently, the regulatory effect of m6A on cuproptosis is multifaceted and complex. At present, the regulatory effect of m6A on cuproptosis has not been thoroughly studied, and further investigation is required to elucidate the precise mechanism of m6A modification in cuproptosis.

In addition to FDX1, additional METTL3-regulated genes, including SOCS2[32], SLC7A11[52], TRIM21[53], EGFR[31], and USP7[54], are involved in HCC progression. Thus, targeting METTL3 with small molecule inhibitors represents a promising therapeutic strategy for HCC. STM2457 is a potent inhibitor of the catalytic activity of METTL3, that reduces AML growth and enhances differentiation and apoptosis[21]. STC-15, the first METTL3 inhibitor in clinical trials[55], exhibits preclinical efficacy against tumor growth via direct anticancer immune effects. However, high intracellular SAM concentrations may compromise the biochemical efficacy of METTL3 inhibitors. On the other hand, the oncogenic role of METTL3 can extend beyond its canonical methyltransferase activity. Proteolysis targeting chimera (PROTAC) targeting the METTL3/METTL14 complex is emerging as an emerging modality, addressing the limitations of METTL3 small-molecule inhibitors. WD6305, a potent and selective PROTAC degrader of the METTL3-METTL14 complex, suppresses m6A modification and the proliferation of AML cells, and promotes apoptosis more effectively than its parent inhibitor does[56]. However, critical questions remain: targeting this essential m6A machinery raises concerns about potential adverse effects, and METTL3 contextually functions as a tumor suppressor. Therefore, a deeper understanding of m6A modification mechanisms in cancer is imperative.

Although our study offers valuable insights into the regulation of cuproptosis in HCC, it has several limitations. First, further studies are warranted to decipher the mechanism by which METTL3 is upregulated in response to cuproptosis. Second, the efficacy of elesclomol-Cu in combination with a METTL3 inhibitor has only been validated in mouse xenograft tumors. In our future work, patient-derived xenograft (PDX) and patient-derived organoid (PDO) models will be constructed and used for further investigation. Third, the potential correlation between cuproptosis and other types of cell death in HCC has not yet been investigated. For example, Wang et al. demonstrated that ferroptosis inducers enhance cuproptosis in primary liver cancer, thereby establishing a close relationship between ferroptosis and cuproptosis[57]. Despite these limitations, our findings shed fresh light on the mechanisms underlying m6A and cuproptosis, establishing a foundation for future and more comprehensive investigations.

Our findings illustrate the crucial role of METTL3 in protecting HCC cells from cuproptotic cell death. Mechanistically, METTL3-mediated m6A modification of FDX1 inhibits FDX1 translation with the assistance of the m6A reader FMR1. Consequently, METTL3 inhibited FDX1 expression in an m6A-FMR1-dependent manner, thereby inhibiting cuprotosis and promoting HCC progression (Fig. 7H). Our study reveals an METTL3-mediated defense mechanism against cuproptosis, indicating that targeting METTL3 in combination with copper ionophores represents a promising therapeutic strategy for HCC.

Methods and materials

Cells, antibodies and chemicals

Hep3B, Huh7, SMMC-7721, HepG2, and LO2 cells (Preserved in Academy of Medical Sciences of Zhengzhou University Translational Medicine platform, Zhengzhou, China) were cultured in the DMEM medium or MEM medium (Servicebio, China) supplemented with 10% fetal bovine serum (FBS and 100 U/mL penicillin–streptomycin. Supplemented with 10% fetal bovine serum (FBS, ExCell Bio, Shanghai, China). The following commercially available antibodies were used for Western blotting: GAPDH (Proteintech, 60004-4-lg), Flag-Tag (Abmart, TT0053), Myc-Tag (Abmart, M20002), METTL3 (Proteintech, 15073-1-AP), METTL14 (Abmart, PC17608), WTAP (Abmart, PA6128), FTO (Abmart, PA2776), ALKBH5 (Proteintech, 16837-1-AP), FDX1 (Abmart, ab108257), FMR1 (Proteintech, 13755-1-AP), DLAT (CST, 12362), YTHDF1 (Abmart, P55973R5), YTHDF2 (Abmart, PY100053), YTHDF3 (Abmart, PS05805), YTHDC1(Proteintech, 14392-1-AP), YTHDC2(Proteintech, 27779-1-AP), Lipoic acid antibody (Abcam, ab58724), m6A antibody (Synaptic Systems, 2002003). Ammonium tetrathiomolybdate (TTM) (Macklin, A828261), Elesclomol (Selleck, STA-4783), STM2457(Glpbio, GC19771), MitoTracker Red CMXRos (Thermo Fisher Scientific, M7512), Z-VAD-FMK (MCE, HY-16658B), 3-Methyladenine (Glpbio, GC10710), Ferrostatin-1 (Glpbio, GC10380).

Tissue specimens and patient information

48 pairs of fresh-frozen HCC and adjacent normal tissue samples obtained from patients who underwent hepatectomy at The First Affiliated Hospital of Zhengzhou University (Zhengzhou, China). All samples were transferred to liquid nitrogen and stored at −80 °C. All samples were approved by the Ethics Committee of the First Affiliated Hospital of Zhengzhou University, and informed consent was obtained from all patients (2024-KY-0327-002).

RNA sequencing

Sequencing service was performed by Wefindbio Biotechnology Co., Ltd. (Wuhan, China). The experimental process was the same as previously described. The cells required for sequencing were from the shMETTL3 group and the control group, with three replicates in each group and treated with elesclomol-Cu for 48 h. Trizol (Takara) reagent was used for RNA extraction, followed by the purification of poly(A) RNA, which was subsequently utilized for cDNA library construction. All samples were sequenced on the MGI DNBSEQ-T7 sequencing platform. Differential gene expression analysis was conducted on two groups using log2FoldChange values in RNA-seq analysis, with a significance threshold of $p < 0.05$. The results were then visually represented using heatmaps and subjected to GSEA for enrichment analysis.

m6A dot blot

The isolated RNA was diluted to 300 ng/μL and denatured at 95 °C for 3 min. 1 μL/2 μL/3 μL of RNA was spotted onto a nylon membrane (Solarbio, China) and the membrane was crosslinked by UV light for 30 min. The samples were washed with SSC solution (Solarbio, China) for 3 min, then blocked with 1% BSA for 1 h. The membrane was hatched with m6A antibody (1:1000) overnight at 4 °C. Finally, the membrane was incubated with diluted secondary anti-rabbit antibody (1:5000) in blocking buffer for 1 h at room temperature, and the RNA amount was imaged using ECL chromogenic solution (Epizyme, China).

RNA extraction and quantitative real-time PCR

Trizol reagent (Servicebio, China) was applied to extract total RNA according to the manufacturer's instructions, and the NanoDrop 2000c instrument (Thermo Fisher, USA) was applied for quantifying RNA

concentration. All-in-One Reverse Transcription Kit (US EVERBRIGHT, China) was used for the reverse transcription of 1 μg total RNA. The quantitative real-time PCR (qRT-PCR) was performed using SYBR Green Kit (Yeason, China) and QuantStudio system (Applied Biosystem, USA). GAPDH was adopted for normalization with the 2−ΔΔct method. The primers were listed in Supplementary Table 1.

Transfection

Lentivirus constructs were purchased from Genechem (Shanghai, China). 2×10^5 cells were cultured in a six-well plate and then transfected with METTL3 or FDX1 overexpression (i.e., METTL3 or FDX1) or knockdown (shMETTL3, shFDX1) recombinant lentivirus after 24 h. Subsequently, cancer cells were cultured in medium containing 2 μg/mL puromycin for 7 days or 500 μg/mL neomycin for 14 days to select stably transfected cells for the next studies. Huh7 and Hep3B cells (1×10^6) were cultured in 96-well plates for 24 h. Then, the cells were incubated with cell medium without FBS overnight. FMR1 in Huh7 and Hep3B cells was silenced by FMR1 siRNA. The shRNA and siRNA sequences were listed in Supplementary Table 2.

Cell growth assay

Cell growth assay was applied with the CCK-8 kit (US EVERBRIGHT, China). Briefly, cells were seeded into a 96-well plate overnight and treated with elesclomol-Cu for 48 h. Then CCK-8 reagents were added to each well, and the plate was incubated in a humidified incubator (37 °C, 5% CO_2) for 1 h. Finally, the absorbance at 450 nm was measured using a microplate reader (SpectraMax M5, Molecular Devices, USA).

Western blot

HCC cells or tissue lysates were extracted using RIPA lysis buffer (Beyotime Biotechnology, China) containing 1% protease inhibitor cocktail (CoWin Biosciences, China) on ice for 30 min. The protein concentration was quantified using the bicinchoninic acid (BCA) assay kit (Solarbio, China) and samples were diluted to the same protein concentration. Equal amounts of proteins were separated by 12.5% or 7.5% sodium dodecyl sulfate–polyacrylamidegel electrophoresis (SDS-PAGE, US EVERBRIGHT, China) and then transferred onto polyvinylidene fuoride (PVDF) membranes (Millipore, USA). The membranes were blocked with 5% non-fat milk for 2 h at room temperature, followed by an overnight incubation with primary antibodies (1:1000) at 4 °C. The next day, the membranes were incubated with HRP-conjugated secondary antibodies (1:5000) for 2 h at room temperature, and an ECL detection system (Amersham Imager 600, GE, USA) was used for visualization.

EdU assay

EdU assay was completed using EdU Cell Proliferation Image Kit (Red Fluorescence) in accordance with the instructions on the operation steps (Uelandy, C6045L). Cells were cultured in the appropriate medium to ensure that they were in an optimal growth state at the beginning of the experiment. Next, medium with the correct concentration of EdU was added to facilitate uptake by the cells undergoing DNA synthesis. The nuclei were stained with a DNA dye to aid in the identification of EdU-labeled cells. Finally, the consequences were observed through a fluorescence microscope.

Cell death assays

Propidium iodide staining and flow cytometry analysis were used to detect cell death. Cells were seeded in six-well plates at a density of 5×10^5 cells per well. On the second day, the cells were treated with the indicated compounds, and then viable and floating dead cells were collected. After washing the cells with PBS, 100 μL of binding buffer was added to each group. Then each group was stained with 10 μL propidium iodide (PI, Yeason, China) and reacted at room temperature for 10 min. Finally, 400 μL of binding buffer was added to each group and analyzed by flow cytometry (Accuri C6, BD, USA) within 1 h.

RNA immunoprecipitation (RIP)

RIP assay was performed according to the manufacturer's instructions of EZ-Magna-RIP kit (Millipore, Billerica, USA). Briefly, cells were lysed by lysis buffer and 10% of the samples were used as input. Then, cell lysates were incubated with magnetic bead protein A/G (Santa Cruz Biotechnology, USA) coated with 6 μg of corresponding antibody overnight at 4 °C. Finally, RNAs were extracted by phenolchloroform RNA extraction and purified for qPCR analysis. IP enrichment was normalized to the input yielded from the same number of cells.

RNA stability assays

HCC cells were seeded into SIX-well plates and treated with actinomycin D(ActD:10 μg/mL, Sigma-Aldrich, USA) at 3, and 6 h, while DMSO (Sangon, Shanghai, China) was added to the negative control group at 0 h. Total RNA was isolated using the phenol-chloroform-ethanol method and then analyzed using qPCR.

MeRIP-qPCR

The m6A modifications on FDX1 mRNA were determined using the Ribo MeRIP m6A Transcriptome Profiling Kit (RiboBio, Canton, China). Briefly, about 50 μg total RNA was extracted and fragmented using RNA fragmentation buffer, and 1/20 of the fragmented RNA was preserved as the input group. Subsequently, 30 μL A/G magnetic beads were prewashed and mixed with 5 μg of anti-m6A antibody (supplied by the kit). The prepared MeRIP reaction buffer was added to the beads, and the mixture was incubated at 4 °C for 2 h followed by washing three times. The conjugate was eluted and purified using the RNA clean & Concentrator™ (Zymo Research, USA) prior to qPCR analysis as described above, washing three times. Relative enrichment of m6A was normalized to the input: % (IP/Input) = $2^{(\text{CT Input-CT IP})} \times 1/20 \times 100$.

Immunofluorescence staining

Frozen sections were baked in 37 °C ovens for 10-20 min, fixed in 4% paraformaldehyde at room temperature for 30 min. After antigen retrieved, blocked with 3% BSA (PBS) for 30 min. Incubated the samples with primary antibody DLAT (Servicebio, China), diluted in 3% BSA at a dilution of 1:1000, overnight at 4 °C. Subsequently, the cells were washed three times with PBS and incubated with fluorescein-labeled secondary antibodies diluted in PBS for 1 h at room temperature. The slide was placed in PBS and washed by shaking on the decolorizing shaker for three times, 5 min each time. Added DAPI dye solution (Servicebio, China) and incubated at room temperature away from light for 10 min. After anti-fluorescence quenching sealing tablets, the samples were observed using a confocal microscope (Nikon Eclipse C1, Japan).

Mice xenograft model

This study received ethical approval from the Animal Protection Committee of Zhengzhou University. We have complied with all relevant ethical regulations for animal use. Female BALB/c nude mice (6–8 weeks of age) were obtained from Jiangsu GemPhaematech and housed in the laboratory animal research center of Zhengzhou University. Mice were housed in a specific pathogen-free (SPF) animal facility. The housing conditions were maintained as follows: temperature at 22 ± 2 °C, relative humidity at 50 ± 10%, and a 12-h light/12-h dark cycle (lights on at 08:00, lights off at 20:00). Each cage (32 cm × 18 cm × 15 cm) housed 3–5 mice of the same sex to avoid aggression. Autoclaved corncob bedding was replaced twice a week to ensure hygiene. Sterilized standard rodent chow and filtered tap water were provided ad libitum. For environmental enrichment, each cage was equipped with a polyvinyl chloride tube (length: 10 cm, diameter: 3 cm) and a sterile wooden chew stick to promote physical activity and reduce stress.

For xenograft models, indicated cells (5×10^6) resuspended in PBS/Matrigel (100 μl, 1:1) were injected subcutaneously into BALB/c nude mice and treated with intraperitoneal ES-Cu (10 mg/kg) once every 3 days. The four groups were as follows: Vector group (Vector), METTL3

overexpression group (OEMETTL3), FDX1 overexpression group (OEFDX1), and METTL3 + FDX1 co-overexpression group (OEMETTL3 + OEFDX1), with 5 mice in each group and a total of 20 mice. Among them, the Vector group (Vector) was the control group. For huh7 xenograft models, Huh7 cells (5×10^6) were injected subcutaneously into BALB/c mice. Mice were randomly grouped after tumor formation and treated with intraperitoneal ES-Cu (10 mg/kg) and/or intraperitoneal STM2457 (30 mg/kg) once every 3 days. The four groups were as follows: Control group (Control), STM2457 group (STM2457), ES-Cu group (ES-Cu), and STM2457 + ES-Cu combined treatment group (STM2457 + ES-Cu), with 5 mice in each group and a total of 20 mice. Tumor size was measured using calipers and its volume was estimated using the following formula: (length × width^2)/2. The experiment was terminated when the maximum tumor volume reached 1500 mm^3. Mice were euthanized at the end of treatment, followed by tumor excision and tumor weight measurement. The collection and analysis of tumor samples were strictly conducted in accordance with the double-blind principle to ensure the objectivity and reliability of the experimental results. Method of random grouping: On the day of enrollment, the animals were numbered from 1 to 20 in ascending order of body weight. Then, an online random number generator (www.random.org) was used to randomly generate 5 numbers for each group. To minimize potential confounding factors, mice in each group were systematically assigned to random locations within the animal facility, all experimental procedures were performed by uniformly trained operators adhering to strict protocols, and the order of treatments and measurements was fully randomized. During the group allocation stage and the experiment conduct stage, the animal experiment operators were aware of the group allocation. During the outcome assessment stage and the data analysis stage, the personnel responsible for data analysis were unaware of the group allocation. The experimental unit was a single mouse. The sample size was 5 mice per group (n = 5), which was decided from previous literature. The total number of mice used in this study was 40. No sample or animal was excluded.

Immunohistochemistry (IHC) staining

Tissues were fixed in 4% paraformaldehyde and embedded in paraffin (Servicebio, China). The tissues were dehydrated, antigen repaired, endogenous peroxidase blocked and sealed, then they were incubated with the corresponding primary antibody (METTL3, 1:150; FDX1, 1:50) at 4 °C overnight. After incubated the tissues with the secondary antibody (1:500) on the second day, the immunohistochemical staining was visualized with diaminobenzidine and hematoxylin (Servicebio, China) counterstain. The protein expression intensity and extent were microscopically determined using the histochemical scoring system (H-score), which is calculated as the sum of the products obtained by multiplying the staining intensity (0, no reactivity; 1, weak; 2, moderate; 3, strong) with the percentage of cells stained at a given intensity (0 to 100). Thus, the score is between 0 and 300.

Bioinformatic analysis

The impact of METTL3 on HCC prognosis was analyzed using web-based tools (GEPIA, Gene Expression Profiling Interactive Analysis, http://gepia.cancer-pku.cn), according to The Cancer Genome Atlas (TCGA) database.

Statistics

All statistical analysis was performed and visualized using GraphPad Prism 8.0 software. Data were presented as mean ± standard deviation (SD) of ≥3 independent experiments. Student's *t* test was used for comparisons between two groups, whereas one-way analysis of variance (ANOVA) was employed for analyses involving more than two groups. $\chi 2$ test was used to analyze categorical variables. Kaplan–Meier curves were used for survival analysis. Statistical significance was considered as p-value < 0.05.

Ethics approval

This study was approved by the ethics committee at the First Affiliated Hospital of Zhengzhou University (2024-KY-0327-002). All ethical regulations relevant to human research participants were followed. All animal experiments are conducted with the approval of the Committee on the Ethics of Animal Experiments of Zhengzhou University. We have complied with all relevant ethical regulations for animal use.

Data availability

The raw sequencing data generated in this study have been deposited in the Sequence Read Archive (SRA) database of the National Center for Biotechnology Information (NCBI) under the BioProject accession number PRJNA1380487. The data are publicly available upon publication. Uncropped Western blot images are provided in Supplementary Fig. 5, attached as Supporting Information to this manuscript. The data supporting the conclusions of this article are included within the article and its additional files. The source data can be found in the Supplementary Data. Other data will be made available from the corresponding author upon reasonable request.

Received: 15 February 2025; Accepted: 29 December 2025;
Published online: 08 January 2026

References

1. Llovet, J. M. et al. Hepatocellular carcinoma. *Nat. Rev. Dis. Prim.* **2**, 16018 (2016).
2. Bray, F. et al. Global cancer statistics 2018: GLOBOCAN estimates of incidence and mortality worldwide for 36 cancers in 185 countries. *CA Cancer J. Clin.* **68**, 394–424 (2018).
3. Hilmi, M. et al. Angiogenesis and immune checkpoint inhibitors as therapies for hepatocellular carcinoma: current knowledge and future research directions. *J. Immunother. Cancer* **7**, 333 (2019).
4. Tsvetkov, P. et al. Copper induces cell death by targeting lipoylated TCA cycle proteins. *Science* **375**, 1254–1261 (2022).
5. Cobine, P. A. & Brady, D. C. Cuproptosis: cellular and molecular mechanisms underlying copper-induced cell death. *Mol. Cell* **82**, 1786–1787 (2022).
6. Tsvetkov, P. et al. Mitochondrial metabolism promotes adaptation to proteotoxic stress. *Nat. Chem. Biol.* **15**, 681–689 (2019).
7. Xie, J., Yang, Y., Gao, Y. & He, J. Cuproptosis: mechanisms and links with cancers. *Mol. Cancer* **22**, 46 (2023).
8. Zhang, C., Huang, T. & Li, L. Targeting cuproptosis for cancer therapy: mechanistic insights and clinical perspectives. *J. Hematol. Oncol.* **17**, 68 (2024).
9. Huang, H., Weng, H. & Chen, J. m(6)A modification in coding and non-coding RNAs: roles and therapeutic implications in cancer. *Cancer Cell* **37**, 270–288 (2020).
10. Frye, M., Harada, B. T., Behm, M. & He, C. RNA modifications modulate gene expression during development. *Science* **361**, 1346–1349 (2018).
11. He, L. et al. Functions of N6-methyladenosine and its role in cancer. *Mol. Cancer* **18**, 176 (2019).
12. He, P. C. & He, C. m(6) A RNA methylation: from mechanisms to therapeutic potential. *EMBO J.* **40**, e105977 (2021).
13. Shi, H., Wei, J. & He, C. Where, when, and how: context-dependent functions of RNA methylation writers, readers, and erasers. *Mol. Cell* **74**, 640–650 (2019).
14. Yang, Y., Hsu, P. J., Chen, Y. S. & Yang, Y. G. Dynamic transcriptomic m(6)A decoration: writers, erasers, readers and functions in RNA metabolism. *Cell Res.* **28**, 616–624 (2018).
15. Zhao, B. S., Roundtree, I. A. & He, C. Post-transcriptional gene regulation by mRNA modifications. *Nat. Rev. Mol. Cell Biol.* **18**, 31–42 (2017).
16. Liu, N. et al. N(6)-methyladenosine-dependent RNA structural switches regulate RNA-protein interactions. *Nature* **518**, 560–564 (2015).
17. Du, K. et al. m(6)A modification of lipoyltransferase 1 inhibits bladder cancer progression by activating cuproptosis. *Oncogene*, https://doi.org/10.1038/s41388-024-03139-5 (2024).

18. Liu, L. et al. Insights into N6-methyladenosine and programmed cell death in cancer. *Mol. Cancer* **21**, 32 (2022).
19. Edupuganti, R. R. et al. N(6)-methyladenosine (m(6)A) recruits and repels proteins to regulate mRNA homeostasis. *Nat. Struct. Mol. Biol.* **24**, 870–878 (2017).
20. Darnell, J. C. et al. FMRP stalls ribosomal translocation on mRNAs linked to synaptic function and autism. *Cell* **146**, 247–261 (2011).
21. Yankova, E. et al. Small-molecule inhibition of METTL3 as a strategy against myeloid leukaemia. *Nature* **593**, 597–601 (2021).
22. Tang, Z. et al. GEPIA: a web server for cancer and normal gene expression profiling and interactive analyses. *Nucleic Acids Res.* **45**, W98–W102 (2017).
23. Sun, Z. et al. AKT1 Phosphorylates FDX1 to promote cuproptosis resistance in triple-negative breast cancer. *Adv. Sci.* **12**, e2408106 (2025).
24. Hao, D., Luo, W., Yan, Y. & Zhou, J. Focus on cuproptosis: exploring new mechanisms and therapeutic application prospects of cuproptosis regulation. *Biomed. Pharmacother.* **178**, 117182 (2024).
25. Zhou, S., Liu, J., Wan, A., Zhang, Y. & Qi, X. Epigenetic regulation of diverse cell death modalities in cancer: a focus on pyroptosis, ferroptosis, cuproptosis, and disulfidptosis. *J. Hematol. Oncol.* **17**, 22 (2024).
26. Brewer, G. METTL3 inhibition enhances anti-tumour immunity. *Nat. Rev. Cancer* **23**, 654 (2023).
27. Zang, Y. et al. METTL3-mediated N(6)-methyladenosine modification of STAT5A promotes gastric cancer progression by regulating KLF4. *Oncogene* **43**, 2338–2354 (2024).
28. Chen, H. et al. RNA N(6)-methyladenosine methyltransferase METTL3 facilitates colorectal cancer by activating the m(6)A-GLUT1-mTORC1 axis and is a therapeutic target. *Gastroenterology* **160**, 1284–1300 e1216 (2021).
29. The RNA Methyltransferase METTL3 promotes oncogene translation. *Cancer Discov.* **6**, 572 (2016).
30. Li, B. et al. METTL3-mediated m(6)A modification of lncRNA TSPAN12 promotes metastasis of hepatocellular carcinoma through SENP1-depentent deSUMOylation of EIF3I. *Oncogene* **43**, 1050–1062 (2024).
31. Wang, L. et al. METTL3-m(6)A-EGFR-axis drives lenvatinib resistance in hepatocellular carcinoma. *Cancer Lett.* **559**, 216122 (2023).
32. Chen, M. et al. RNA N6-methyladenosine methyltransferase-like 3 promotes liver cancer progression through YTHDF2-dependent posttranscriptional silencing of SOCS2. *Hepatology* **67**, 2254–2270 (2018).
33. Chen, H. et al. METTL3 inhibits antitumor immunity by targeting m(6) A-BHLHE41-CXCL1/CXCR2 axis to promote colorectal cancer. *Gastroenterology* **163**, 891–907 (2022).
34. Guirguis, A. A. et al. Inhibition of METTL3 results in a cell-intrinsic interferon response that enhances antitumor immunity. *Cancer Discov.* **13**, 2228–2247 (2023).
35. Zeng, C., Huang, W., Li, Y. & Weng, H. Roles of METTL3 in cancer: mechanisms and therapeutic targeting. *J. Hematol. Oncol.* **13**, 117 (2020).
36. Su, W. et al. METTL3 regulates TFRC ubiquitination and ferroptosis through stabilizing NEDD4L mRNA to impact stroke. *Cell Biol. Toxicol.* **40**, 8 (2024).
37. Wu, D., Spencer, C. B., Ortoga, L., Zhang, H. & Miao, C. Histone lactylation-regulated METTL3 promotes ferroptosis via m6A-modification on ACSL4 in sepsis-associated lung injury. *Redox Biol.* **74**, 103194 (2024).
38. Zhang, J. et al. Excessive miR-25-3p maturation via N(6)-methyladenosine stimulated by cigarette smoke promotes pancreatic cancer progression. *Nat. Commun.* **10**, 1858 (2019).
39. Wang, Q. et al. METTL3-mediated m(6)A modification of HDGF mRNA promotes gastric cancer progression and has prognostic significance. *Gut* **69**, 1193–1205 (2020).
40. Du, M. et al. MiR-33a suppresses proliferation of NSCLC cells via targeting METTL3 mRNA. *Biochem. Biophys. Res. Commun.* **482**, 582–589 (2017).
41. Cui, X. et al. Cross talk between RNA N6-methyladenosine methyltransferase-like 3 and miR-186 regulates hepatoblastoma progression through Wnt/beta-catenin signalling pathway. *Cell Prolif.* **53**, e12768 (2020).
42. Wei, W., Huo, B. & Shi, X. miR-600 inhibits lung cancer via downregulating the expression of METTL3. *Cancer Manag Res.* **11**, 1177–1187 (2019).
43. He, H., Wu, W., Sun, Z. & Chai, L. MiR-4429 prevented gastric cancer progression through targeting METTL3 to inhibit m(6)A-caused stabilization of SEC62. *Biochem. Biophys. Res. Commun.* **517**, 581–587 (2019).
44. Cai, X. et al. HBXIP-elevated methyltransferase METTL3 promotes the progression of breast cancer via inhibiting tumor suppressor let-7g. *Cancer Lett.* **415**, 11–19 (2018).
45. Du, Y. et al. SUMOylation of the m6A-RNA methyltransferase METTL3 modulates its function. *Nucleic Acids Res.* **46**, 5195–5208 (2018).
46. Xiong, J. et al. Lactylation-driven METTL3-mediated RNA m(6)A modification promotes immunosuppression of tumor-infiltrating myeloid cells. *Mol. Cell* **82**, 1660–1677 e1610 (2022).
47. Sun, H. L. et al. Stabilization of ERK-Phosphorylated METTL3 by USP5 Increases m(6)A Methylation. *Mol. Cell* **80**, 633–647 e637 (2020).
48. Li, Y. et al. METTL3 acetylation impedes cancer metastasis via fine-tuning its nuclear and cytosolic functions. *Nat. Commun.* **13**, 6350 (2022).
49. Quan, Y. et al. Tumor cuproptosis and immune infiltration improve survival of patients with hepatocellular carcinoma with a high expression of ferredoxin 1. *Front. Oncol.* **13**, 1168769 (2023).
50. Sun, B. et al. FDX1 downregulation activates mitophagy and the PI3K/AKT signaling pathway to promote hepatocellular carcinoma progression by inducing ROS production. *Redox Biol.* **75**, 103302 (2024).
51. Sun, L. et al. Lactylation of METTL16 promotes cuproptosis via m(6)A-modification on FDX1 mRNA in gastric cancer. *Nat. Commun.* **14**, 6523 (2023).
52. Zhang, C. et al. METTL3 inhibition promotes radiosensitivity in hepatocellular carcinoma through regulation of SLC7A11 expression. *Cell Death Dis.* **16**, 9 (2025).
53. Jin, X. et al. METTL3 confers oxaliplatin resistance through the activation of G6PD-enhanced pentose phosphate pathway in hepatocellular carcinoma. *Cell Death Differ.* **32**, 466–479 (2025).
54. Li, Y. et al. METTL3 facilitates the progression of hepatocellular carcinoma by modulating the m6A level of USP7. *Am. J. Transl. Res.* **13**, 13423–13437 (2021).
55. Li, G., Chen, W., Liu, D. & Tang, S. Recent advances in medicinal chemistry strategies for the development of METTL3 inhibitors. *Eur. J. Med. Chem.* **290**, 117560 (2025).
56. Du, W. et al. Discovery of a PROTAC degrader for METTL3-METTL14 complex. *Cell Chem. Biol.* **31**, 177–183 e117 (2024).
57. Wang, W. et al. Ferroptosis inducers enhanced cuproptosis induced by copper ionophores in primary liver cancer. *J. Exp. Clin. Cancer Res.* **42**, 142 (2023).

Acknowledgements

This work was supported by the Fund for Clinical Medical Scientists in Henan Province (HNCMS202412); the Fund for Distinguished Young Scholars of Medical Science and Technology Innovation in Henan Province (YXKC2022033); the Central Plains Young Elite Talents program; the Fund for Scientific Research and Innovation Team of The First Affiliated Hospital of Zhengzhou University (QNCXTD2023018); the National Natural Science Foundation of China (82322053 and 32370819); Guangzhou Science and

Technology Program Project (2025A04J7154); the Postdoctoral Fellowship Program of China Postdoctoral Science Foundation (GZC2022434); and the Open Funds of State Key Laboratory of Oncology in South China.

Author contributions

Dan Liao, Jiao Zhao and Ting Sun conceptualized and supervised this study. Qian Jiang, Chen Peng, and Wenhao Mao performed the majority of the experiments. Zhuo Yu, Yadan Feng, Yurui Li and Jialin Zhu collected and analyzed the data. Dan Liao and Jiao Zhao reviewed the manuscript and performed text corrections. Qian Jiang and Ting Sun wrote the manuscript. Ting Sun provided financial support. All authors read and approved the final manuscript.

Competing interests

The authors declare no competing interests.

Additional information

Supplementary information The online version contains supplementary material available at https://doi.org/10.1038/s42003-025-09497-4.

Correspondence and requests for materials should be addressed to Jiao Zhao, Dan Liao or Ting Sun.

Peer review information *Communications Biology* thanks Yu-Man Tsui and the other, anonymous, reviewer(s) for their contribution to the peer review of this work. Primary Handling Editors: Bibekanand Mallick and Kaliya Georgieva.